JOURNAL OF SPACECRAFT AND ROCKETS
Vol. 42, No. 6, November–December 2005

Navier–Stokes Solutions with Finite Rate Ablation for Planetary Mission Earth Reentries

Yih-Kanq Chen* and Frank S. Milos†
NASA Ames Research Center, Moffett Field, California 94035-1000

A formulation of finite rate ablation surface boundary conditions, including oxidation, nitridation, and sublimation of carbonaceous material with pyrolysis gas injection, based on surface species mass conservation, has been developed. These surface boundary conditions are discretized and integrated with a Navier–Stokes solver. This numerical procedure can predict aerothermal heating, chemical species concentration, and carbonaceous material ablation rates over the heat-shield surface of reentry space vehicles. Two finite rate gas–surface interaction models, based on the work of Park and of Zhluktov and Abe, are considered. Three test cases are studied. The stream conditions of these test cases are typical for Earth reentry from a planetary mission with both oxygen and nitrogen fully or partially dissociated inside the shock layer. Predictions from both gas–surface interaction models are compared with those obtained by using chemical equilibrium ablation tables. Stagnation point convective heat fluxes predicted by using Park's finite rate model are usually below those obtained from chemical equilibrium tables and Zhluktov and Abe's model. Recession predictions from Zhluktov and Abe's model are usually lower than those obtained from Park's model and from chemical equilibrium tables. The effect of species mass diffusion on the predicted ablation rate is also examined.

Nomenclature

B'	=	dimensionless mass blowing rate, $\dot{m}/\rho_e u_e C_m$
C_i	=	mass fraction for species i
C_m	=	Stanton number for mass transfer
$(C-i)$	=	adatom i, O or N
c_p	=	specific heat, J/Kg · K
D_i	=	diffusion coefficient for species i, m^2/s
$\bar{D}$	=	bifurcation diffusion coefficient, m^2/s
E	=	total energy per unit volume, J/m^3
F	=	nonlinear equation, Eq. (24), or $P_0/\sqrt{(2\pi m_i kT)}$
f_i	=	diffusion factor of species i
h	=	Planck's constant, J · s, or enthalpy, J/kg
J	=	mass diffusion flux, kg/m^2 · s
K_i	=	equilibrium constant
K_t	=	thermal conductivity of translation temperature, W/m · K
K_v	=	thermal conductivity of vibration temperature, W/m · K
k	=	Boltzmann constant, J/K
k_f	=	forward reaction rate, Eq. (18)
k_r	=	backward reaction rate, Eq. (18)
M	=	molecular weight, kg/mole
m_i	=	mass of species i, kg
$\dot{m}$	=	mass flux, kg/m^2 · s
$\hat{N}_i$	=	Eq. (12)
p	=	pressure, N/m^2
p_E	=	saturated vapor pressure, N/m^2
Q_{T-v}	=	rate of translation and vibration energy exchange, W/m^3
q_{conv}	=	convective heat flux, W/m^2
q_v	=	heat flux due to species diffusion, W/m^2
R	=	universal gas constant, J/kmol · K
R_b	=	base radius, m
R_c	=	corner radius, m
R_n	=	nose radius, m
r_i	=	reaction rate; Eq. (14)
$\dot{S}$	=	recession rate, m/s
T	=	temperature, K
t	=	time, s
u	=	fluid velocity, m/s
v_s	=	species diffusion velocity, m/s
v_w	=	mass injection velocity, m/s
w	=	species source term in Eq. (1), kg/m^3 · s
x	=	Cartesian coordinate system, m
Z_i	=	bifurcation diffusion quantity of species i; Eq. (4)
α	=	surface absorptance
β	=	efficiency of gas–surface interaction
ε	=	surface emissivity
ε_i	=	factor in ith heterogeneous reaction
η	=	general body-fitted coordinate system normal to surface, m
Θ_i	=	surface coverage concentration of species i
Θ^0	=	free surface concentration
λ	=	blowing reduction parameter in Eq. (12)
μ	=	viscosity, N · s/m^2
$\hat{\mu}_i$	=	defined in Eq. (4)
$\bar{v}_i$	=	$\sqrt{(kT_w/2\pi m_i)}$, m/s
ρ	=	density, kg/m^3
σ	=	Stefan–Boltzmann constant, W/m^2 · K^4
τ	=	shear stress, N/m^2
χ	=	mole fraction
∇	=	gradient, m^{-1}

Subscripts

c	=	char
E	=	chemical equilibrium
e	=	boundary-layer edge
g	=	pyrolysis gas
i	=	species or direction component
j	=	surface species, or direction component
s	=	gas species or stagnation point
v	=	virgin or vibrational energy
w	=	wall

Presented as Paper 2004-2270 at the AIAA 37th Thermophysics Conference, Portland, OR, 28 June–1 July 2004; received 14 July 2004; revision received 6 December 2004; accepted for publication 16 December 2004.

*Aerospace Engineer, Mail Stop 234-1, Thermal Protection Materials and Systems Branch.

†Ceramic Engineer, Mail Stop 234-1, Thermal Protection Materials and Systems Branch. Senior Member AIAA.

Introduction

THE Charring Material Thermal Response and Ablation Program (CMA)[1] was developed by Aerotherm Corporation in the 1960s. The Fully Implicit Ablation and Thermal Response Program[2] (FIAT) was developed at NASA Ames Research Center in the 1990s. Both FIAT and CMA solve the same one-dimensional internal energy balance and decomposition equations, coupled with the ablating surface energy balance condition, to simulate the response of ablative heat shields in hypersonic flows. The aerothermal heating environment required for CMA and FIAT computations is calculated by a flow simulation code. The surface boundary conditions of the flow simulation can be either nonablating or ablating. If nonablating surface conditions are used, a blowing reduction parameter λ is introduced in the material response code to account for the blockage effect from ablation products.[3] If ablating surface conditions are used, iterations between the flow solver and the material response code are performed to obtain the appropriate ablating surface conditions, such as the procedures used for the heat-shield design for Mars Pathfinder[4] and Stardust.[5] In most CMA and FIAT computations, the surface recession rates are determined by solving the surface energy balance with precalculated B' tables. The B' tables were generated using the Aerotherm Chemical Equilibrium program (ACE)[6] or the Multicomponent Ablation Thermochemistry code (MAT)[7] and assuming that the ablating surface and ambient gas are in chemical equilibrium. This approach has been widely used for many engineering applications, and the predictions provide satisfactory accuracy with minimum computational cost. In recent years, the Two-Dimensional Implicit Thermal Response and Ablation (TITAN) program[8] was developed and integrated with the Gauss–Seidel Implicit Aerothermodynamic Navier–Stokes with Thermochemical Surface boundary conditions (GIANTS) code,[9–12] using a loosely coupled method to perform a thermal response and shape change simulation for charring materials.[13,14] The surface thermochemistry procedure implemented in the TITAN code is based on the same pregenerated B' tables used in CMA and FIAT.

Chemical equilibrium is a special condition of the general chemical nonequilibrium condition. The convective heating and surface recession rate predicted by the chemical equilibrium surface chemistry is usually reasonably conservative and is considered to be a best alternative when the nonequilibrium computation is too expensive or unlikely to be achieved. The B' tables are established by solving the chemical equilibrium relations and the elemental species balance equations with thin-film transfer theory. If the chemical species concentrations, such as a chemical nonequilibrium shock layer with the presence of radiation, must be precisely defined in the flow simulation, then the chemical equilibrium surface conditions will never be adequate. Attempts were made to modify B' tables to include some nonequilibrium effects and to better fit ablation data,[6,15] but the gas-phase nonequilibrium ablation products cannot be determined without a finite rate simulation. The nonequilibrium ablating surface can be simulated using a finite rate model similar to that used in the gas-phase chemistry. The viscous shock-layer solutions of airflow over a blunt body with finite rate ablating carbon surface were studied by Zhluktov and Abe.[16] A comparison of surface chemical kinetic models for an ablative graphite nose tip at high pressure was made by Havstad and Ferencz.[17] The solution with finite rate ablating surface conditions along the stagnation streamline for a carbon-phenolic heat shield was studied by Park and Ahn[18] to examine the effect of nonequilibrium surface chemistry on surface ablation and shock-layer radiation. Similar computations, using a full Navier–Stokes solver with the finite rate ablating surface conditions, have not been performed for multidimensional simulation of hypersonic flow with carbon-phenolic heat-shield interactions.

The full Navier–Stokes computation of finite rate surface ablation requires detailed knowledge of complicated interactions between the solid surface and the ambient gas, and between the ablation products and the ambient gas. This is expected to be computationally intensive because a large number of chemical species and reactions must be simulated. However, because computer storage devices, CPU speeds, and multiprocessor technologies are significantly improved on an ongoing basis, hardware limitations may no longer be a concern.

The major obstacle of finite rate simulation is that for many heat-shield materials the interactions between the surface and gas are not well understood. The purpose of this work is to obtain the full Navier–Stokes solutions with finite rate surface ablation conditions for carbon and carbon-phenolic materials, using available surface kinetic models, and to perform parametric studies to understand their performance and enable future improvement for the simulation of planetary mission Earth reentries. Carbon and carbon-phenolic materials are selected as the heat-shield materials in this study because their interactions with air are better understood. As more is known about the interactions of other heat-shield materials with ambient gases, this same computational methodology can be applied for other ablators. Because the entire flowfield is to be solved, the thin-film theory assumption made in establishing the B' tables is no longer needed, and all of the problems associated with the approximation of transfer coefficient and recovery enthalpy are avoided.

In this work, the formulation of finite rate ablation surface boundary conditions, including recombination, oxidation, nitridation, and sublimation of carbonaceous materials with pyrolysis gas, is developed based on species mass conservation. Two kinetic models for gas–surface interactions are studied. One was developed by Park,[19–21] and the other is the work of Zhluktov and Abe.[16] Park's model does not consider the recombination reactions, and Zhluktov's model ignores the nitridation reaction. Thus, there is a significant need to characterize finite rate atomic nitrogen surface reactions. The gas–gas interactions are based on the work of Park. These boundary conditions are discretized and integrated with the GIANTS code to predict the aerothermal heating, the gas-phase chemical species concentrations, and the carbon ablation rate. The concentrations of all surface chemical species are determined from gas–surface chemical reactions balanced by mass transfer rate. The surface recession rate is thus obtained as part of the flowfield solution.

In a typical computation using B' tables, the surface recession is computed from the material response code. The surface temperature and pyrolysis gas injection rate are determined through time-dependent, fully coupled iterations between the flow solver and the material code. The iteration strategy between the flow and material response codes is different for a finite rate ablation surface than for a chemical equilibrium surface.[4,5] For simplicity, a simplified steady-state ablation assumption is adopted in the energy balance. This is to avoid a complicated fully coupled flow/solid simulation and to focus on the study of finite rate surface ablation at a certain trajectory point. A discussion of time-dependent fully coupled iteration between a flow solver and a material thermal response code is not in the scope of the study and will be presented in a separate paper.

The computation model developed in this work can be used to simulate carbon-phenolic or carbon ablation during Earth reentry from a planetary mission. Three test cases are presented. The first case is a graphite test model in the arcjet stream, the second is a lightweight phenolic impregnated carbon ablator (PICA) at the Stardust reentry peak heating conditions, and the third is a carbon-phenolic heat shield at the peak heating point of a proposed Mars sample return (MSR) Earth entry vehicle (EEV). In case 1, the predicted graphite mass blowing rates are compared with arcjet data. All three cases have peak stagnation point pressures below 1 atm. In cases 2 and 3, both oxygen and nitrogen are fully dissociated through the entire shock layer. Under these stream conditions, sublimation is not the only dominant process for surface recession. Surface oxidation and nitridation play equally important roles. These results are typical for NASA's sample return missions. The details of the computational procedure and the results of test cases are presented and discussed in the following sections.

Navier–Stokes Solver

The Navier–Stokes solver GIANTS is used to estimate the hypersonic aerothermal heating distribution over a blunt body. The governing equations used in the code, as developed by Lee,[22] may be characterized as representing a flowfield in thermo-chemical nonequilibrium. The GIANTS code solves the time-dependent

conservation equations of mass, momentum, and energy for the chemical and thermal nonequilibrium flowfield. The species mass conservation equation is given by[11]

$$\frac{\partial \rho_s}{\partial t} + \frac{\partial}{\partial x_j}(\rho_s u_j) = -\frac{\partial}{\partial x_j}(\rho_s v_{sj}) + w_s \tag{1}$$

The total momentum conservation is written as

$$\frac{\partial}{\partial t}(\rho u_i) + \frac{\partial}{\partial x_j}(\rho u_i u_j) = -\frac{\partial \tau_{ij}}{\partial x_j} \tag{2}$$

and the vibrational and total energy equations are written as

$$\frac{\partial E_v}{\partial t} + \frac{\partial}{\partial x_j}(E_v u_j) = -\frac{\partial}{\partial x_j}(q_{vj}) + Q_{T-v}$$

$$\frac{\partial E}{\partial t} + \frac{\partial}{\partial x_j}[(E+p)u_j] = -\frac{\partial}{\partial x_j}(q_j + q_{vj})$$

$$-\frac{\partial}{\partial x_j}(u_i \tau_{ij}) - \sum_{s=1}^{n} \frac{\partial}{\partial x_j} v_{sj} h_s \tag{3}$$

These equations are discretized using the implicit flux-split finite volume method. The discretized equations may be solved by a block-tridiagonal matrix inversion using Gauss–Seidel line relaxation with alternating sweeps in the backward and forward directions (see Refs. 9 – 11). This technique has been shown to yield steady-state results efficiently. There is a total of 14 gas-phase species: CO_2, CO, N_2, O_2, NO, C_2, C_3, CN, H_2, HCN, C, N, O, and H. Five of the species are for air, and the rest are for ablation products. The gas-phase chemical reactions implemented in the GIANTS code are from the work of Park.[21] The total number of reactions is 19, including 9 dissociation reactions and 10 exchange reactions.

The dissociation reactions are as follows:

1) $CO_2 + M \leftrightarrow CO + O + M$
2) $CO + M \leftrightarrow C + O + M$
3) $N_2 + M \leftrightarrow N + N + M$
4) $O_2 + M \leftrightarrow O + O + M$
5) $NO + M \leftrightarrow N + O + M$
6) $C_2 + M \leftrightarrow C + C + M$
7) $C_3 + M \leftrightarrow C_2 + C + M$
8) $CN + M \leftrightarrow C + N + M$
9) $H_2 + M \leftrightarrow H + H + M$

The exchange reactions are as follows:

10) $NO + O \leftrightarrow N + O_2$
11) $N_2 + O \leftrightarrow NO + N$
12) $CO + O \leftrightarrow O_2 + C$
13) $CO_2 + O \leftrightarrow O_2 + CO$
14) $CO + C \leftrightarrow C_2 + O$
15) $CO + N \leftrightarrow CN + O$
16) $N_2 + C \leftrightarrow CN + N$
17) $CN + O \leftrightarrow NO + C$
18) $CN + C \leftrightarrow C_2 + N$
19) $HCN + H \leftrightarrow CN + H_2$

The mass diffusion models implemented in the GIANTS code include the constant Lewis number Le, the constant Schmidt number Sc, and the bifurcation approximation. These models are an approximation of the full multicomponent mass diffusion. The effect of the mass diffusion model on the ablation prediction is studied later in this paper. For the bifurcation model, the species mass diffusion rate is defined as[6]

$$J_i = -\rho \bar{D}(\hat{\mu}_1/\hat{\mu}_2)\nabla Z_i \tag{4}$$

where

$$Z_i = \frac{C_i}{f_i \hat{\mu}_1}, \qquad \hat{\mu}_1 = \sum \frac{C_i}{f_i}, \qquad \hat{\mu}_2 = M \sum \frac{C_i f_i}{M_i}$$

For the constant Schmidt number, $\rho D_i = \mu/Sc$, and for the constant Lewis number,

$$\rho D_i = Le[(K_t + K_v)/c_p]$$

The total convective heat flux to the surface is given as

$$q_{\text{conv}} = -K_t \nabla T_t - K_v \nabla T_v + \sum h_i \rho D_i \nabla \chi_i \tag{5}$$

Gas–Surface Interactions

Two finite rate gas–surface interaction models are considered in the present study. The first one was developed by Park,[19,20] and the second one was the work of Zhluktov and Abe. Park's model has all of the carbon consuming reactions, but does not consider the recombination reactions. Zhluktov and Abe's model has no nitridation reaction, but includes some surface recombination reactions.

Park's Model

Three kinds of gas–surface interactions for the carbonaceous ablating surface are considered. The gas–solid reactions include oxidation, Eqs. (6) and (7), and nitridation, Eq. (8). Following the assumption made in Park and Ahn's[18] and Park's work the surface catalysis reactions are assumed to be negligibly small for both oxygen atom and nitrogen atom recombination at the ablating surface. The sublimation of carbon produces C_3; C_1 and C_2 are also neglected. The species C_5 and C_7 are not included because the entry conditions studied in this work have a stagnation point pressure of less than 1 atm. Thus, the carbon mass blowing rates due to gas–surface interaction are

$$\dot{m}_1 = \rho C_O \bar{\nu}_O \beta_O \left(M_C/M_O\right) \qquad \left(O + C_{(s)} \rightarrow CO\right) \tag{6}$$

$$\dot{m}_2 = 2\rho C_{O_2} \bar{\nu}_{O_2} \beta_{O_2} \left(M_C \big/ M_{O_2}\right) \qquad \left(O_2 + 2C_{(s)} \rightarrow 2CO\right) \tag{7}$$

$$\dot{m}_3 = \rho C_N \bar{\nu}_N \beta_N (M_C/M_N) \qquad \left(N + C_{(s)} \rightarrow CN\right) \tag{8}$$

$$\dot{m}_4 = \rho\left(C_{C_3}, E - C_{C_3}\right)\bar{\nu}_{C_3}\beta_{C_3} \qquad \left(3C_{(s)} \rightarrow C_3\right) \tag{9}$$

$$\dot{m}_c = \dot{m}_1 + \dot{m}_2 + \dot{m}_3 + \dot{m}_4 = \rho_{(s)}\dot{S} \tag{10}$$

Here, $\bar{\nu}_i$ is defined as $\sqrt{(kT_w/2\pi m_i)}$. The total surface mass blowing rate $\dot{m}_c$ and the surface recession rate $\dot{S}$ can be computed from the total carbon mass loss. Here, β_O is given as $0.63\exp(-1160/T_W)$, β_N is assumed to be 0.3 (Ref. 23), and β_{O2} has been measured by various investigators[24]; the latter was varied from 0 to 0.5 in the present work. The vaporization coefficient β_{C3} is varied between 0.1 and 1 with little difference seen in the result[20] and is set to 1 in this work. The equilibrium C_3 concentration in Eq. (9) is computed from the saturated vapor pressure. The saturated carbon vapor pressure P_E for carbon phenolic is expressed as[20]

$$p_E = 6.27 \times 10^{15} \exp(-90{,}908/T_w)$$

and for carbon as

$$p_E = 5.19 \times 10^{15} \exp(-90{,}845/T_w)$$

Species mass conservation at the surface is written as

$$-\rho D_i \nabla \chi_i + \rho v_w C_i = \hat{N}_i + \dot{m}_g C_{i,g} \tag{11}$$

The first term on the left-hand side is mass transfer through diffusion, and the second term is mass transfer due to convection. On the right-hand side are the source terms due to gas–surface interaction and pyrolysis gas injection. For graphite or pure carbon heat-shield materials, the pyrolysis gas injection rate $\dot{m}_g$ is zero. Here, the source term $\hat{N}_i$ is defined as

$$\hat{N}_{CO} = \dot{m}_1(M_{CO}/M_C) + \dot{m}_2(M_{CO}/M_C), \qquad \hat{N}_{CN} = \dot{m}_3(M_{CN}/M_C)$$

$$\hat{N}_{C_3} = \dot{m}_4, \qquad \hat{N}_N = -\dot{m}_3(M_N/M_C), \qquad \hat{N}_O = -\dot{m}_1(M_O/M_C)$$

$$\hat{N}_{O_2} = -\dot{m}_2\left(M_{O_2}\big/2M_C\right) \tag{12}$$

and $\hat{N}_i = 0$ for $i = CO_2$, N_2, NO, C_2, and C.

Zhluktov and Abe's Model

The following surface-kinetic model is suggested in the work of Zhluktov and Abe[16]:

1) $O + (C) <==> (C - O)$
2) $O_2 + 2(C) <==> 2(C - O)$
3) $O_2 + (C) <==> (C - O) + O$
4) $CO_2 + (C) <==> (C - O) + CO$
5) $(C - O) <==> CO + (C)$
6) $O + (C - O) <==> CO_2 + (C)$
7) $2(C - O) <==> CO_2 + 2(C)$
8) $(C) <==> C + (C)$
9) $2(C) <==> C_2 + 2(C)$
10) $3(C) <==> C_3 + 3(C)$
11) $N + (C) <==> (C - N)$
12) $(C - N) + N <==> N_2 + (C)$

The corresponding reaction rates and constants are listed in the Appendix.

Based on global mass balance, the following equation for total mass blowing is expressed:

$$\rho v_w = \dot{m}_c + \dot{m}_g \tag{13}$$

After discretizing the species conservation [Eq. (11) for Park's model and Eq. (A11) for Zhluktov and Abe's model], the resulting nonlinear equations can be solved through iterations. Species concentrations $C_{i,w}$ and velocity v_w at each surface grid point are updated in each sweep (both backward and forward) until a steady-state flow solution is reached.

The surface temperature T_w, pyrolysis gas injection rate $\dot{m}_g$, and species concentrations of pyrolysis gas $C_{i,g}$ have to be obtained through time-dependent global iterations between a material thermal response code and a flow simulation code. The current study mainly focuses on developing the finite rate ablation boundary conditions for a flow solver and examining the available gas–surface interaction models. The results presented here are the steady-state Navier–Stokes solutions without performing time-dependent global iterations. Thus, assumptions on pyrolysis gas conditions and surface temperature have to be made. The pyrolysis gas injection rate is specified based on previous similar computations, and its surface species concentrations are calculated by assuming chemical equilibrium before being injected into the main stream. The surface temperature is specified based on the measurement, or is computed by solving the simplified surface energy balance with the assumption of steady-state ablation adopted in Ref. 16. The simplified surface energy balance equation is written as

$$-q_{\text{conv}} = \sigma \varepsilon T_w^4 + \dot{m} h_w^{\text{gas}} - \dot{m}_g h_g \tag{14}$$

The surface temperature at each surface grid point can be obtained by solving Eqs. (5) and (14).

Results and Discussion

The general finite rate carbon-phenolic ablation model without pyrolysis gas injection ($\dot{m}_g/\dot{m}_c = 0$) can be used to simulate graphite ablation. The first test case is a study of the interaction between a graphite model and an arcjet stream, conducted in the Interactive Heating Facilities at NASA Ames Research Center. The stream total enthalpy is estimated to be approximately 27 MJ/kg, and the measured stagnation point pressure is 0.80 atm. Other calculated freestream quantities are listed in Table 1. In this arc stream, oxygen is fully dissociated and nitrogen is partially dissociated.

The graphite model is a 10-deg, one-half-angle sphere cone with nose radius R_n of 1.905 cm. The geometry and computational grid for this test model are shown in Fig. 1. Surface temperature distribution was measured using an infrared camera and pyrometers. Thus, instead of solving the simplified surface energy balance, Eq. (14), the surface temperature profile is specified based on the measurement. The surface temperature and pressure profiles are shown in Fig. 2.

Predicted carbon mass blowing rate distributions over the model surface are shown in Fig. 3. The dark solid line is the prediction based on the chemical equilibrium surface condition. The Navier–Stokes solutions with a chemical equilibrium ablation surface condition are computed using the procedure presented in Ref. 5. The solid lines are the results of Park's surface kinetics with and without the nitridation surface reaction ($N + C_{(s)}$), and the dotted line is the computation using the surface reactions proposed by Zhluktov and Abe. The B' tables used in the chemical equilibrium surface calculation were generated with the assumption of $Le = 1$. To be consistent with the chemical equilibrium surface calculation, the computations with finite rate surface conditions were also performed with $Le = 1$.

Around the nose-tip region, the mass blowing rate predicted by the chemical equilibrium surface conditions is about 10% lower than predicted by Park's finite rate condition with the nitridation reaction. The chemical equilibrium surface prediction gradually declines and, in the relatively low-temperature conical section, approaches the prediction of Park's finite rate conditions without nitridation. In the nose-tip region, the ablation rate predicted by Zhluktov and Abe's model is about the same as predicted by Park's model without

Table 1 Calculated freestream conditions for test case 1

Property	Value
Velocity	5354 m/s
Density	0.003 kg/m^3
Temperature	1428 K
Mass concentrations	
C_{O_2}	0.0
C_{N_2}	0.6169
C_{NO}	0.0046
C_N	0.1212
C_O	0.2573

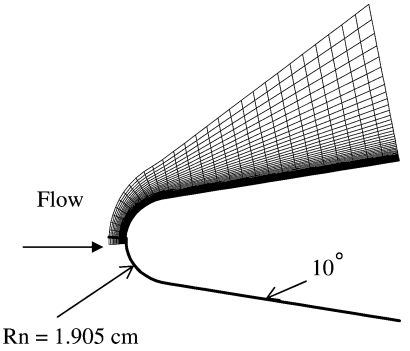

Fig. 1 Geometry and computational grid for case 1.

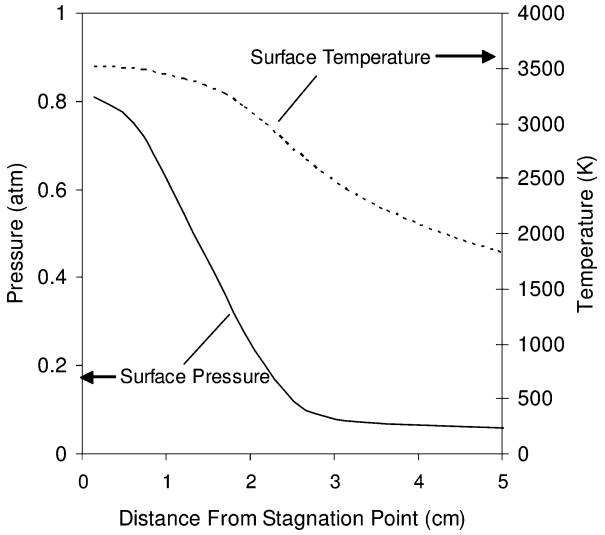

Fig. 2 Surface temperature and pressure distributions along graphite surface.

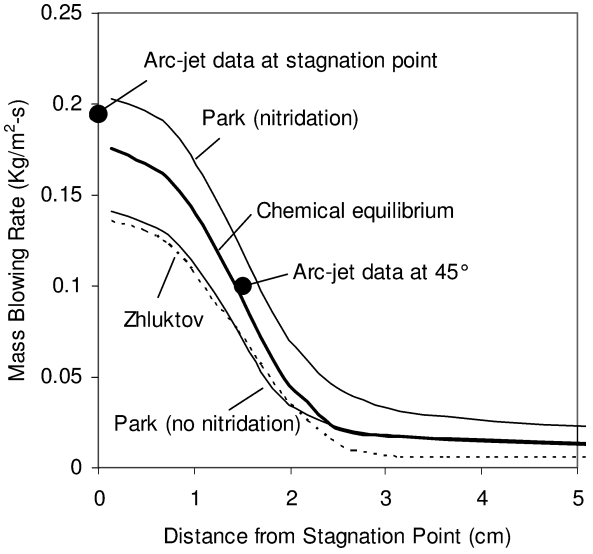

Fig. 3 Predicted carbon mass blowing rate distributions for various surface chemistry conditions (case 1).

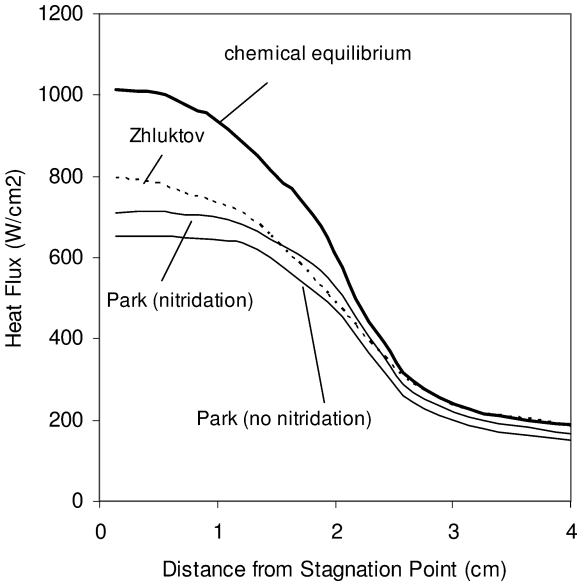

Fig. 4 Comparison of convective heat flux predictions for various surface chemistry conditions (case 1).

nitridation. In the conical region, however, the prediction with Zhluktov and Abe's model becomes relatively low and is approximately 50% below the chemical equilibrium model. Surface recession data are measured at stagnation point and at ±45 deg from the stagnation point. The symbols in Fig. 3 are the mean graphite mass blowing rates of a 30-s heat pulse. Without the nitridation reaction, both finite rate modes underpredict the mass blowing rate by about 25% at the stagnation point, and by about 20% at 45 deg from the stagnation point. The difference between the prediction using Park's model with nitridation and arcjet data is less than 5% at the stagnation point and is about 20% at 45 deg from the stagnation point.

If the surface and its ambient gas do reach a condition of chemical equilibrium, there is no dissociated nitrogen available near the graphite surface. As a result, the surface nitridation reaction proposed in Park's model can never occur, and the prediction is insensitive to the nitridation efficiency. However, in a chemical condition that is far from equilibrium, such as that studied in this case, some dissociated nitrogen does exist at the graphite surface. The predicted mass blowing is, therefore, sensitive to the efficiency of nitridation reaction defined in Park's model. (The work conducted by Park and Bogdanoff shows that the surface nitridation reaction may be important, but more studies are required to fully understand the reaction rate.) It was found that the $O_2 + C_{(s)}$ oxidation reaction has no effect on the ablation prediction because there is no significant availability of oxygen molecules near the surface.

A comparison of predicted surface heat fluxes is presented in Fig. 4. The heating predictions using Park's finite rate model with and without nitridation (solid lines) are quite close. This is because the net energy exchange due to the surface nitridation reaction is small. However, the predictions are approximately 30% lower than the heat flux predicted by the chemical equilibrium surface (dark solid line). In the nose-tip region, the heating prediction of Zhluktov and Abe's model is 20% lower than chemical equilibrium model, and, in the conical section, Zhluktov and Abe's model comes closer to the chemical equilibrium at the surface.

Figure 5 presents the chemical species distributions along the stagnation streamline for Park's finite rate model with nitridation. Solid lines are the predictions with $Le = 1$ and dotted lines are those with the bifurcation diffusion model. The results indicate that the bifurcation diffusion model tends to give lower mass diffusion rates than $Le = 1$. To examine the effect of mass diffusion on the prediction of the surface mass blowing rate, Park's finite rate surface computations with nitridation were conducted using three mass diffusion models: $Le = 1$, $Sc = 0.7$, and bifurcation. The results are shown in Fig. 6. As expected, the predicted mass blowing rates

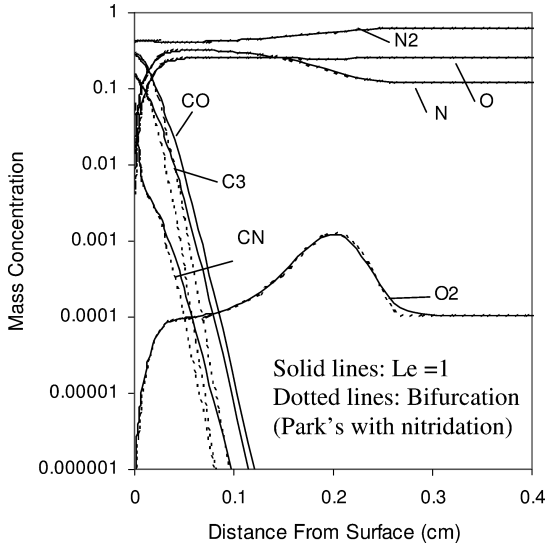

Fig. 5 Chemical species distributions along the stagnation streamline for different mass diffusion models (case 1).

are sensitive to the diffusion model implemented in the computation. The prediction of $Le = 1$ gives the highest rate, $Sc = 0.7$ is the second, and the bifurcation model gives the lowest mass blowing rate. The result is consistent with the species concentration profiles shown in Fig. 5.

The second case is a simulation of hypersonic flow interacting with a PICA heat shield at the estimated Stardust reentry peak heating conditions. PICA has the same chemical composition as carbon phenolic. With a density of 240 kg/m^3, however, it is much lighter than fully dense carbon phenolic (density = 1440 kg/m^3). The aeroshell of the Stardust reentry vehicle is a 60-deg one-half-angle spherical cone with a nose radius of 0.2286 m, a base radius of 0.4064 m, and a corner radius of 0.02 m. The freestream velocity is 11,137 m/s, the density is 0.000234 kg/m^3, and the temperature is 238 K. The geometry and computational grid for the Stardust aeroshell are shown in Fig. 7.

In addition to the assumptions made in energy balance of Eq. (14), based on previous experience,[5] the pyrolysis gas injection rate can be approximated by $\dot{m}_g/\dot{m}_c = (\rho_v/\rho_c - 1)$. Thus, the pyrolysis gas injection rate is around 21% of the carbon char mass blowing rate. The pyrolysis gas itself is assumed to be at chemical equilibrium

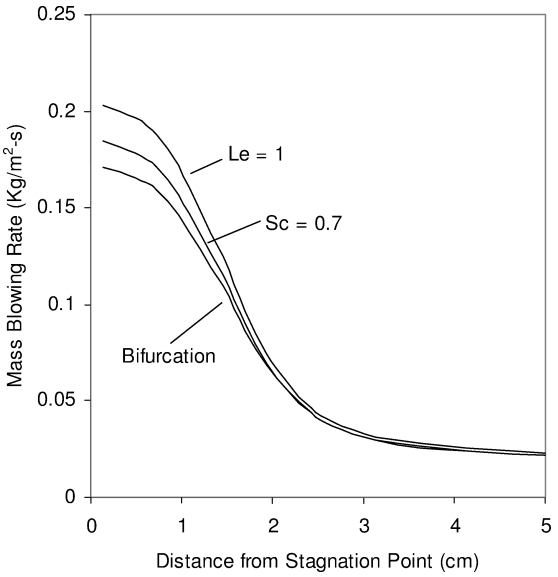

Fig. 6 Effect of the mass diffusion model on predicted mass blowing rate distributions (case 1).

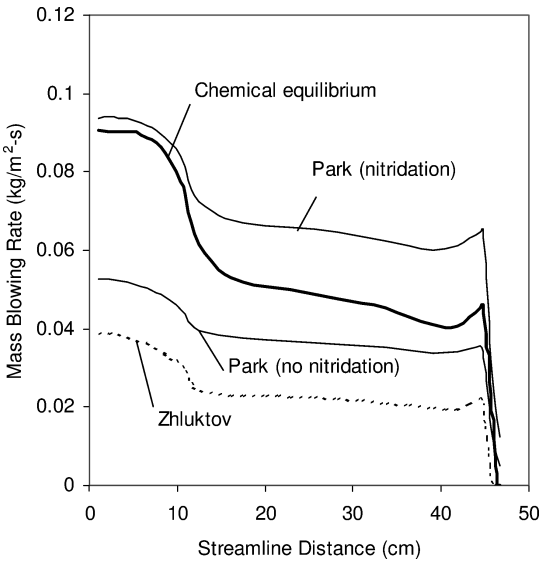

Fig. 8 Predicted total mass blowing rate distributions for various surface chemistry conditions (case 2).

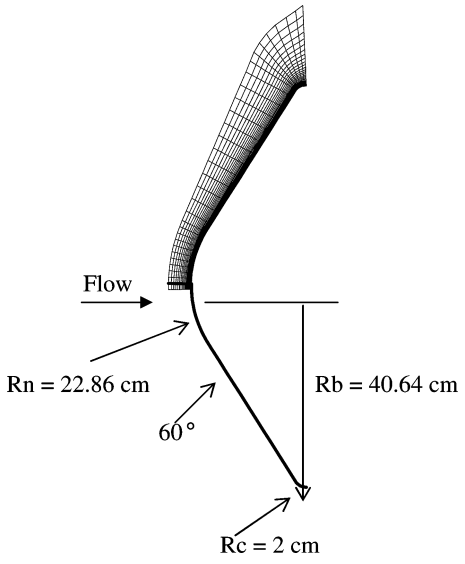

Fig. 7 Geometry and computational grid for Stardust aeroshell.

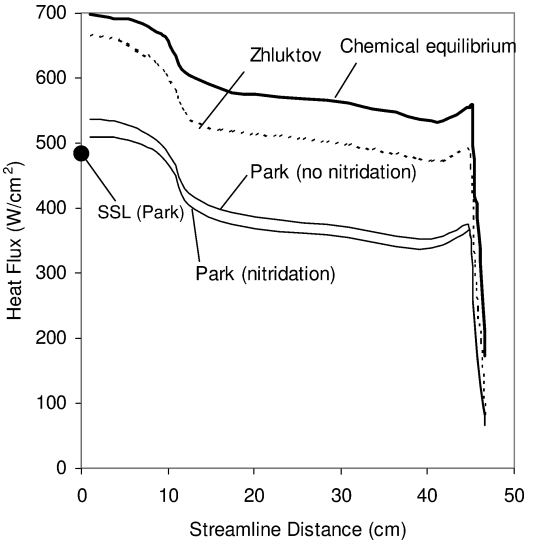

Fig. 9 Comparison of convective heat flux predictions using different surface chemistry conditions (case 2).

before injection into the stream. The equilibrium species concentrations of pyrolysis gas are computed using MAT and are mostly CO, H_2, and H.

Gas radiation from the shock layer, which is no more than 10% of the total heat flux at the Stardust peak heating point, is not included in this study. The ablation products may affect the net radiation reaching the ablating surface. The present computation, however, ignores this possible effect on the radiation. For simplicity, the ion species are also not considered in the simulation. Previous experience has shown that the effect of ion species on the predicted convective heating for Stardust entry conditions is less than 5% (Ref. 5).

The predicted total mass blowing rates, including char and pyrolysis gas, are presented in Fig. 8. The solid lines are the predictions using Park's finite rate conditions with and without the nitridation reaction. The dotted line is the prediction based on Zhluktov and Abe's model, and the dark solid line represents the solution based on chemical equilibrium at the surface. Again, for consistency with the chemical equilibrium surface calculations, the finite rate surface predictions shown in Fig. 8 were performed with $Le = 1$. Around the nose-tip region, the prediction using the chemical equilibrium surface assumption is slightly lower than that using Park's finite rate surface with nitridation. In the conical region, the prediction by using chemical equilibrium surface assumption declines at a higher rate than the finite rate models. The ablation rate based on Zhluktov and Abe's model is the lowest. This is because nitrogen is fully dissociated through the entire shock layer, and Zhluktov and Abe's model has no nitridation reaction to compete with surface oxidation. The $O_2 + C_{(s)}$ reaction has no contribution to the surface ablation, because there is no molecular oxygen (O_2) available in the boundary layer. However, the nitridation reaction has a very significant effect on the predicted ablation rate. The ablation rate calculated using Park's model with nitridation is about 80% higher than that without nitridation.

Figure 9 shows the predicted convective heat fluxes. The chemical equilibrium surface prediction is almost 35% higher than Park's finite rate surface predictions over the entire forebody heatshield surface. The difference between the heating predictions of Park's model with and without nitridation is small. Zhluktov and Abe's model gives the convective heating around 10% below the chemical equilibrium. This is due to the energy-releasing nitrogen recombination and other nonablating surface reactions included in Zhluktov and Abe's model. The stagnation streamline solution computed in Park's study[19] is almost identical to the current

Navier–Stokes finite rate prediction using Park's surface model with nitridation.

The interaction between nitrogen atoms and carbonaceous materials is not well understood. The work conducted by Goldstein[25] did not find the formation of CN around ablating graphite. The CN molecules are likely to undergo the exchange reaction with nitrogen atoms and produce nitrogen molecules and carbon ($N + CN \rightarrow N_2 + C$). Then, carbon may condense back on to the ablating wall ($C \rightarrow C_{(s)}$). The combination of nitridation and the two preceding reactions is equivalent to the nitrogen surface catalytic process ($N + N_{(s)} \rightarrow N_2$). For this reason, the surface kinetic model used by Zhluktov and Abe[16] does not even consider the formation of CN. Instead, it includes the nitrogen recombination reaction. For a very high-speed reentry, such as Stardust and MSR EEV, a large portion of stream enthalpy is stored in nitrogen atoms. An appropriate kinetic model for nitrogen and carbon surface interactions is essential for accurate prediction of heat flux and recession. At present, however, insufficient data are available in this area.

The chemical species concentrations along the stagnation streamline are presented in Fig. 10. The species concentrations presented are those computed using Zhluktov and Abe's model (dotted lines) and Park's model without nitridation (solid lines). Both nitrogen and oxygen are fully dissociated along the stagnation streamline. As expected, Zhluktov and Abe's model predicted higher N_2 concentration at the surface because of the nitrogen recombination reaction. The CO concentrations predicted by both models are about the same. The CO_2 and C_3 concentrations computed using Zhluktov and Abe's model are much higher than those of Park's model.

The effect of the diffusion model on the predicted mass blowing rate for Park's finite rate model with nitridation is shown in Fig. 11. The results were obtained using the diffusion models with $Le = 1$, $Sc = 0.7$, and bifurcation, respectively. The prediction using the bifurcation model has the lowest mass blowing rate, and that using $Le = 1$ has the highest rate.This trend is exactly the same as seen in the first case.

The third test case is the simulation of the hypersonic flowfield over a fully dense carbon-phenolic heat shield at the peak heating point of the proposed MSR EEV trajectory. The forebody heat shield is a 60-deg one-half-angle spherical cone with a nose radius of 0.352 m, a base radius of 0.45 m, and a corner radius of 0.02 m. The freestream velocity is 10,100 m/s, the density is 0.0006634 kg/m^3, and the temperature is 255 K. The stream velocity at the peak heating point and the geometry of the MSR EEV aeroshell are similar to those of Stardust. The EEV is slightly larger, and the freestream density is almost three times as high as that of Stardust. The geometry and computational grid for this test case are shown in Fig. 12. The gas radiation from the shock layer and the ion species are not considered in the simulation. In the previous MSR EEV heat-shield

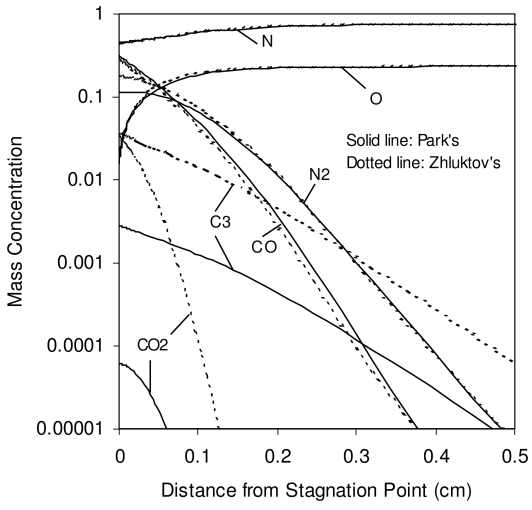

Fig. 10 Species concentrations along the stagnation streamline for Park and Zhluktov and Abe models (case 2).

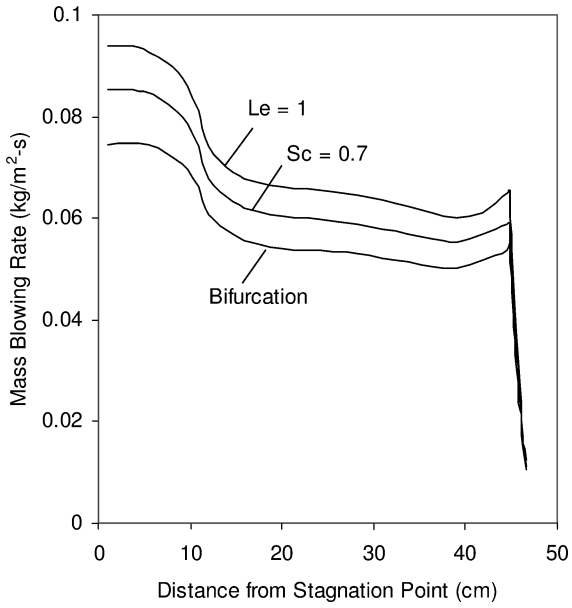

Fig. 11 Effect of mass diffusion model on predicted mass blowing rate (case 2).

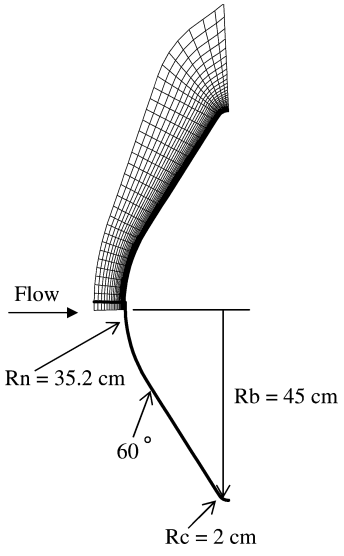

Fig. 12 Geometry and computational grid for case 3.

analysis,[13] it was found that the total surface recession is small and that the char mass blowing rate is approximately the same as, or less than, the pyrolysis gas blowing rate. To avoid a complicated flow/solid fully coupled simulation, the assumption of $\dot{m}_g/\dot{m}_c = 1$ was selected for solving the simplified energy balance with a steady-state ablation condition [Eq. (14)]. Thus, 50% of the ablation product comes from the pyrolysis gas.

The predicted total mass blowing rate distributions (char and pyrolysis gas) are presented in Fig. 13. The solid lines are the predictions using Park's finite rate conditions with and without the nitridation reaction. The dotted line is that of Zhluktov and Abe's model, and the dark solid line is the prediction based on the chemical equilibrium surface assumption. The finite rate computations are again performed with $Le = 1$. The difference between the predictions using chemical equilibrium and using Park's model with nitridation is less than 15%. It was found that the nose-tip surface was in the low sublimation region if the chemical equilibrium surface was used. However, it stayed in the diffusion-controlled region if the finite rate surface models were used. The ablation rate of Park's model without nitridation is 40% lower than with nitridation. Zhluktov and Abe's model again gives the lowest mass blowing rate.

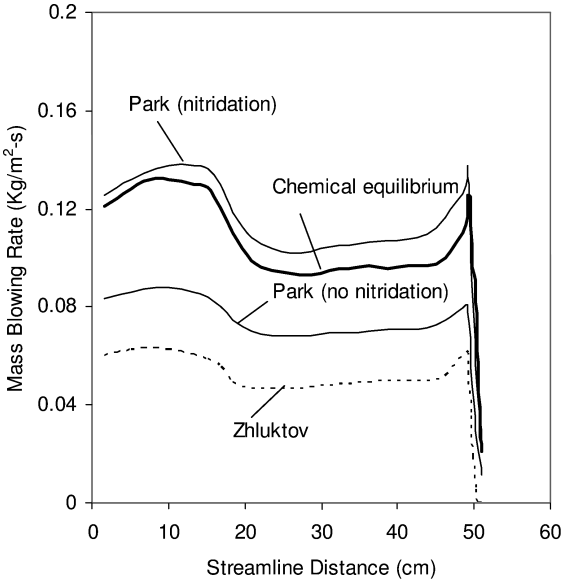

Fig. 13 Predicted total mass blowing rate distributions for various surface chemistry conditions (case 3).

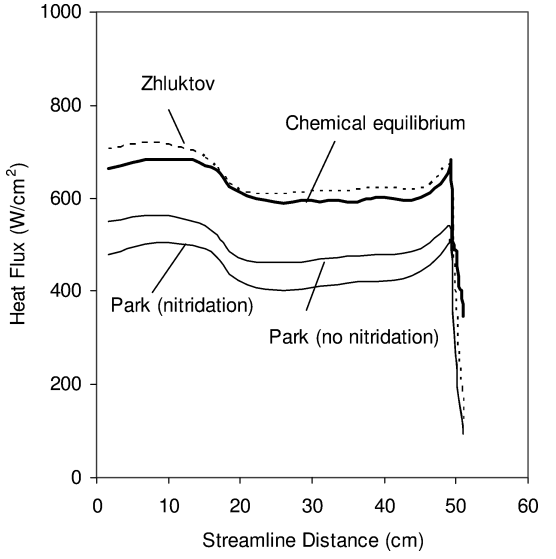

Fig. 14 Comparison of convective heat flux predictions using different surface chemistry conditions (case 3).

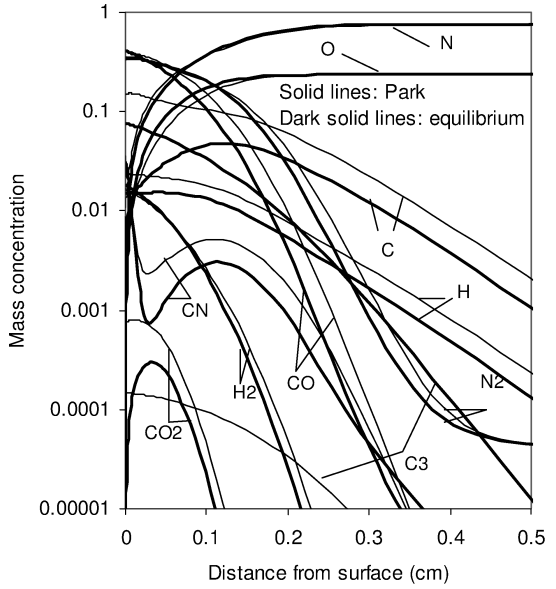

Fig. 15 Chemical species concentrations for Park's model with nitridation and equilibrium models along stagnation streamline for case 3.

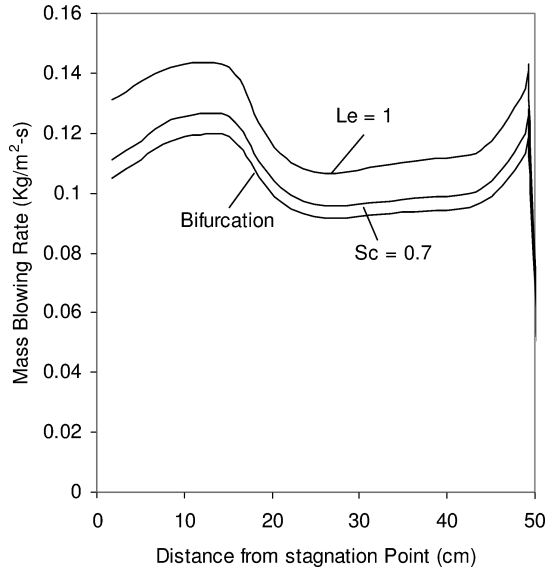

Fig. 16 Effect of mass diffusion model on predicted mass blowing rate distributions for Park's finite rate model with nitridation (case 3).

Figure 14 shows the predicted surface heat fluxes. The heating distribution calculated on the assumption of a chemical equilibrium surface is slightly lower than Zhluktov and Abe's prediction for a finite rate surface. The chemical equilibrium surface prediction is about 30–35% higher than Park's finite rate surface prediction. Park's model with nitridation predicted a lower heat flux than without nitridation because the nitridation reaction significantly increases the ablation rate, but releases only a small amount of energy.

The surface nitridation reaction ($N + C_{(s)} \rightarrow CN$) releases 0.35 eV of energy, and the surface nitrogen recombination reaction ($N + N_{(s)} \rightarrow N_2$) releases 9.8 eV. If the nitridation reactions are replaced by recombination reactions, such as those proposed in Zhluktov and Abe's model, the predicted surface heat flux may increase significantly, and the ablation rate would be reduced. A similar situation occurs between oxidation ($O + C_{(s)} \rightarrow CO + 3.74$ eV) and oxygen recombination ($O + O_{(s)} \rightarrow O_2 + 5.08$ eV) (Ref. 26), but the difference in energy release is not as great.

The chemical species concentrations along the stagnation streamline for Park's model with nitridation and with a chemical equilibrium surface are shown in Fig. 15. The C_3 concentration predicted from the chemical equilibrium surface is at least two orders of magnitude higher than Park's model predicted. The CO, CN, and CO_2 concentrations of the chemical equilibrium surface are far less than those predicted in Park's model. The ablation rates predicted by the chemical equilibrium surface and Park's model with nitridation are about the same at the stagnation area, but apparently they are not a result of the same surface reactions. The effect of the diffusion model on the predicted mass blowing rate is shown in Fig. 16. The results presented are for the three models, $Le = 1$, $Sc = 0.7$, and bifurcation. The prediction with bifurcation still has the lowest mass blowing rate, and that with $Le = 1$ has the highest rate.

Conclusions

The formulation of the finite rate surface boundary conditions for carbonaceous material ablation with pyrolysis gas injection was developed for the Navier–Stokes equation solver GIANTS, to predict the surface recession and the convective heat flux of carbon and carbon-phenolic heat shields on reentry space vehicles. Solutions for three test cases, using two kinetic models for gas–surface interactions, were successfully obtained and compared with results for chemical equilibrium ablation surface conditions.

In case 1, without the nitridation reaction, both kinetic models underpredict the graphite mass blowing rate by more than 20% compared with arcjet data. The predicted mass blowing rate using Park's model with nitridation is within 5% of arcjet data at the stagnation point and is about 20% higher than data at 45 deg from the stagnation point.

Generally speaking, the convective heat fluxes predicted from Park's model are lower than those from Zhluktov and Abe's model, and the mass blowing rates predicted from Park's model are higher than those from Zhluktov and Abe's model. For all three test cases, Park's model, with a constant surface nitridation efficiency of 0.3, predicted much higher mass blowing rates than those predicted without the nitridation reaction. However, the surface nitridation reaction has only a small impact on the predicted convective heat flux.

Park's model does not have any nonablating surface recombination reactions. This model, therefore, can lead to underprediction of the convective heat flux. Zhluktov and Abe's model does not include the nitridation reaction. If nitridation proves to be important, their model can under predict the ablation rate. The parametric studies show that prediction of mass blowing rates is sensitive to the mass diffusion model. Species mass diffusion and gas–surface reactions are equally important for determining the surface ablation rate and the convective heat flux.

More experimental data on the gas–surface interactions are needed to validate the accuracy of these finite rate models. To ensure that both the ablation rate and the convective heat flux are accurately predicted, it is important to use more complex species mass diffusion models and to include appropriate nitridation and nitrogen recombination reactions in a nonequilibrium surface model.

Appendix: Reaction Rates and Constants for Zhluktov's Model

The corresponding reaction rates for Zhluktov and Abe's model are as follows:

$$r_1 = k_{f1}\left(p\chi_{\mathrm{O}}\Theta^0 - \Theta_{\mathrm{O}}/K_1\right)$$

$$r_2 = k_{r2}\left[K_2 p\chi_{\mathrm{O}_2}(\Theta^0)^2 - (\Theta_{\mathrm{O}})^2\right]$$

$$r_3 = k_{f3}\left(p\chi_{\mathrm{O}_2}\Theta^0 - p\chi_{\mathrm{O}}\Theta_{\mathrm{O}}/K_3\right)$$

$$r_4 = k_{f4}\left(p\chi_{\mathrm{CO}_2}\Theta^0 - p\chi_{\mathrm{CO}}\Theta_{\mathrm{O}}/K_4\right)$$

$$r_5 = k_{f5}\left(\Theta_{\mathrm{O}} - p\chi_{\mathrm{CO}}\Theta^0\big/K_5\right)$$

$$r_6 = k_{f6}\left(p\chi_{\mathrm{O}}\Theta_{\mathrm{O}} - p\chi_{\mathrm{CO}_2}\Theta^0\big/K_6\right)$$

$$r_7 = k_{f7}\left[(\Theta_{\mathrm{O}})^2 - p\chi_{\mathrm{CO}_2}(\Theta^0)^2\big/K_7\right]$$

$$r_8 = k_{r8}\Theta^0(K_8 - p\chi_{\mathrm{C}})$$

$$r_9 = k_{r9}(\Theta^0)^2(K_9 - p\chi_{\mathrm{C}_2})$$

$$r_{10} = k_{r10}(\Theta^0)^3\left(K_{10} - p\chi_{\mathrm{C}_3}\right)$$

$$r_{11} = k_{f11}\left(p\chi_N\Theta^0 - \Theta_N/K_{11}\right)$$

$$r_{12} = k_{r12}\left(K_{12}p\chi_N\Theta_N - p\chi_{\mathrm{N}_2}\Theta^0\right) \tag{A1}$$

It is assumed that two possibilities exist for K_1 and K_{11}. The first is mobile adsorption:

$$1/K_i = B(kT/P_0)\left(2\pi m_i kT\big/h^2\right)^{\frac{1}{2}}\exp\left(-T_{d_i}\big/T\right)\mathrm{atm} \tag{A2}$$

and the second is immobile adsorption:

$$1/K_i = (kT/P_0)\left(2\pi m_i kT\big/h^2\right)^{\frac{3}{2}}\exp\left(-T_{d_i}\big/T\right)\mathrm{atm} \tag{A3}$$

where $i = 1$ or 11, $P_0 = 1.01325 \times 10^5$ Pa, and $B = 3.5 \times 10^{19}$ m^{-2}. Equation (A2) is used in this work. K8 is expressed as follows:

$$K_8 = 9.30 \times 10^7 \exp(-85{,}334/T) \tag{A4}$$

The equilibrium constants K_1–K_{12} are not independent. They are related via gas-phase equilibrium constants of corresponding dissociation processes:

$$K_2 = (K_1)^2 K_{\mathrm{O}_2}$$

$$K_3 = K_1 K_{\mathrm{O}_2}$$

$$K_4 = K_1 K_{\mathrm{CO}_2}$$

$$K_5 = K_8/(K_1 K_{\mathrm{CO}})$$

$$K_6 = K_8\Big/\left(K_1 K_{\mathrm{CO}} K_{\mathrm{CO}_2}\right)$$

$$K_7 = K_8\Big/\left[(K_1)^2 K_{\mathrm{CO}} K_{\mathrm{CO}_2}\right]$$

$$K_9 = (K_8)^2\Big/K_{\mathrm{C}_2}$$

$$K_{10} = (K_8)^3\Big/\left(K_{\mathrm{C}_2} K_{\mathrm{C}_3}\right)$$

$$K_{12} = 1\Big/\left(K_{11} K_{\mathrm{N}_2}\right) \tag{A5}$$

The recommended expressions for necessary forward or backward reaction rate constants are as follows:

$$k_{f1} = \varepsilon_1 F_{\mathrm{O}}$$

$$k_{r2} = \varepsilon_2 B(kT/h)\exp(-T_{a2}/T)$$

$$k_{f3} = \varepsilon_3 F_{\mathrm{O}_2}\exp\left(-T_{a3}/T\right)$$

$$k_{f4} = \varepsilon_4 F_{\mathrm{CO}_2}$$

$$k_{f5} = \varepsilon_5 B(kT/h)\exp(-T_{a5}/T)$$

$$k_{f6} = \varepsilon_6 F_{\mathrm{O}}\exp(-T_{a6}/T)$$

$$k_{f7} = \varepsilon_7 B(kT/h)\exp(-T_{a7}/T)$$

$$k_{r8} = \varepsilon_8 F_{\mathrm{C}}$$

$$k_{r9} = \varepsilon_9 F_{\mathrm{C}_2}$$

$$k_{r10} = \varepsilon_{10} F_{\mathrm{C}_3}$$

$$k_{f11} = \varepsilon_{11} F_{\mathrm{N}}$$

$$k_{r12} = \varepsilon_{12} F_{\mathrm{N}_2}\exp(-T_{a12}/T) \tag{A6}$$

where

$$F_i = P_0\Big/\sqrt{2\pi m_i kT}$$

$$\varepsilon_1 = 1, \quad \varepsilon_2 = 0.0008, \quad \varepsilon_3 = 1, \quad \varepsilon_4 = 0.9$$

$$\varepsilon_5 = 0.1, \quad \varepsilon_6 = 0.8, \quad \varepsilon_7 = 1, \quad \varepsilon_8 = 0.24$$

$$\varepsilon_9 = 0.5, \quad \varepsilon_{10} = 0.023, \quad \varepsilon_{11} = 1, \quad \varepsilon_{12} = 1$$

$$T_{d1} = 45{,}000, \qquad T_{d11} = 36{,}600, \qquad T_{a2} = 30{,}800$$

$$T_{a3} = 14{,}200, \qquad T_{a12} = 76{,}600, \qquad T_{a5} = 40{,}000$$

$$T_{a6} = 2000, \qquad T_{a7} = 40{,}000$$

The preceding reaction rate constants are adopted from the work of Havstad and Ferencz.[17]

The rates of species production on the surface are

$$\dot{m}_{\mathrm{O}} = (-r_1 + r_3 - r_6)M_{\mathrm{O}}$$

$$\dot{m}_{\mathrm{CO}} = (r_4 + r_5)M_{\mathrm{CO}}$$

$$\dot{m}_{\mathrm{CO_2}} = (-r_4 + r_6 + r_7)M_{\mathrm{CO_2}}$$

$$\dot{m}_{\mathrm{C}} = r_8 M_{\mathrm{C}}$$

$$\dot{m}_{\mathrm{C_2}} = r_9 M_{\mathrm{C_2}}$$

$$\dot{m}_{\mathrm{C_3}} = r_{10} M_{\mathrm{C_3}}$$

$$\dot{m}_{\mathrm{NO}} = 0$$

$$\dot{m}_{\mathrm{CN}} = 0$$

$$\dot{m}_{\mathrm{N}} = (-r_{11} - r_{12})M_{\mathrm{N}}$$

$$\dot{m}_{\mathrm{O_2}} = (-r_2 - r_3)M_{\mathrm{O_2}}$$

$$\dot{m}_{\mathrm{N_2}} = r_{12} M_{\mathrm{N_2}} \tag{A7}$$

For a stationary regime, we have

$$\dot{m}_{(\mathrm{C-O})} = (r_1 + 2r_2 + r_3 + r_4 - r_5 - r_6 - 2r_7)M_{\mathrm{O}} = 0$$

$$\dot{m}_{(\mathrm{C-N})} = (r_{11} - r_{12})M_N = 0 \tag{A8}$$

When these expressions are used, the total surface mass blowing rate is

$$\dot{m} = \sum \dot{m}_i = M_{\mathrm{C}}(r_5 + r_6 + r_7 + r_8 + 2r_9 + 3r_{10}) \tag{A9}$$

The sum of surface coverage concentrations is equal to 1:

$$\Theta_{\mathrm{O}} + \Theta_{\mathrm{N}} + \Theta^0 = 1 \tag{A10}$$

Species conservation at the surface is written as

$$-\rho D_i \nabla \chi_i + \rho v_w C_i = \dot{m}_i + \dot{m}_{\mathrm{g}} C_{i,\mathrm{g}} \tag{A11}$$

The total number of unknowns is 13:

$$\left[\chi_{\mathrm{O}}, \chi_{\mathrm{O_2}}, \chi_{\mathrm{N}}, \chi_{\mathrm{N_2}}, \chi_{\mathrm{C}}, \chi_{\mathrm{C_2}}, \chi_{\mathrm{C_3}}, \chi_{\mathrm{CN}}, \chi_{\mathrm{CO}}, \chi_{\mathrm{CO_2}}, \Theta_{\mathrm{O}}, \Theta_{\mathrm{N}}, \Theta^0\right]$$

References

[1]*User's Manual: Aerotherm Charring Material Thermal Response and Ablation Program*, Aerotherm Div., Acurex Corp., Mountain View, CA, 1987.

[2]Chen, Y.-K., and Milos, F. S., "Ablation and Thermal Analysis Program for Spacecraft Heatshield Analysis," *Journal of Spacecraft and Rockets*, Vol. 36, No. 3, 1999, pp. 475–483.

[3]Kays, W. M., and Crawford, M. E., *Convective Heat and Mass Transfer*, 2nd ed., McGraw–Hill, New York, 1980, pp. 355–357.

[4]Chen, Y.-K., Henline, W. D., and Tauber, M. E., "Mars Pathfinder Trajectory Based Heating and Ablation Calculations," *Journal of Spacecraft and Rockets*, Vol. 32, No. 2, 1995, pp. 225–230.

[5]Olynick, D. R., Chen, Y.-K., and Tauber, M. E., "Aerothermodynamics of the Stardust Sample Return Capsule," *Journal of Spacecraft and Rockets*, Vol. 36, No. 3, 1999, pp. 442–462.

[6]*User's Manual: Aerotherm Chemical Equilibrium Computer Program*, Aerotherm Div., Acurex Corp., Mountain View, CA, 1981.

[7]Milos, F. S., and Chen, Y.-K., "Comprehensive Model for Multi-Component Ablation Thermochemistry," AIAA Paper 97-0141, Jan. 1997.

[8]Chen, Y.-K., and Milos, F. S., "Two-Dimensional Implicit Thermal Response and Ablation Program for Charring," *Journal of Spacecraft and Rockets*, Vol. 38, No. 4, 2001, pp. 473–481.

[9]MacCormack, R. W., "Current Status of Numerical Solutions of the Navier–Stokes Equation," AIAA Paper 85-0032, Jan. 1985.

[10]Candler, G. V., and MacCormack, R. W., "Hypersonic Flow Past 3-D Configuration," AIAA Paper 87-0480, June 1987.

[11]Candler, G. V., "Computation of Hypersonic Ionized Flows in Chemical and Thermal Nonequilibrium," AIAA Paper 88-0511, Jan. 1988.

[12]Chen, Y.-K., Henline, W. D., Stewart, D. A., and Candler, G. V., "Navier–Stokes Solutions with Surface Catalysis for Martian Atmospherical Entry," *Journal of Spacecraft and Rockets*, Vol. 30, No. 1, 1993, pp. 32–42.

[13]Chen, Y.-K., and Milos, F. S., "Thermal Response Modeling System for a Mars Sample Return Vehicle," Thermal and Fluid Analysis Workshop, NASA CP-2002-211783, Sept. 2001.

[14]Chen, Y.-K., Milos, F. S., Reda, D. C., and Stewart, D. A., "Graphite Ablation and Thermal Response Simulation Under Arc-Jet Flow Conditions," AIAA Paper 2003-4042, June 2003.

[15]Beck, R. A. S., Johnson, P. A., Gorden, M. L., and Laub, B., "IUS Nozzle Materials Thermal Characterization," Aerotherm Div., Acurex Corp., Acurex Final Rept. FR-84-21/ATD, Mountain View, CA, Aug. 1984.

[16]Zhluktov, S. V., and Abe, T., "Viscous Shock-Layer Simulation of Airflow past Ablating Blunt Body with Carbon Surface," *Journal of Thermophysics and Heat Transfer*, Vol. 13, No. 1, 1999, pp. 50–59.

[17]Havstad, M. A., and Ferencz, R. M., "Comparison of Surface Chemical Kinetic Models for Ablative Reentry of Graphite," *Journal of Thermophysics and Heat Transfer*, Vol. 16, No. 4, 2002, pp. 508–515.

[18]Park, C., and Ahn, H. K., "Stagnation-Point Heat Transfer for Pioneer-Venus Probes," *Journal of Thermophysics and Heat Transfer*, Vol. 13, No. 1, 1999, pp. 33–41.

[19]Park, C., "Calculation of Stagnation-Point Heating Rates Associated with Stardust Vehicle," AIAA Paper 2005-190, Jan. 2005.

[20]Park, C., "Stagnation-Point Ablation of Carbonaceous Flat Disks, Part 1: Theory," *AIAA Journal*, Vol. 21, No. 11, 1983, pp. 1588–1594.

[21]Park, C., "Review of Chemical Kinetic Problems of Future NASA Missions, 1: Earth Entries," *Journal of Thermophysics and Heat Transfer* Vol. 7, No. 3, 1993, pp. 385–398.

[22]Lee, J. H., "Basic Governing Equations for the Flight Regimes of Aeroassisted Orbital Transfer Vehicles," *Thermal Design of Aeroassisted Orbital Transfer Vehicles*, edited by H. F. Nelson, Vol. 96, Progress in Astronautics and Aeronautics, AIAA, New York, 1985, pp. 3–53.

[23]Park, C., and Bogdanoff, D. W., "Shock Tube Measurement of Coefficient of Reaction of Nitrogen Atoms and Solid Carbon," AIAA Paper 2003-0158, Jan. 2003.

[24]Park, C., *Nonequilibrium Hypersonic Aerothermodynamics*, Wiley, New York, 1990, p. 350.

[25]Goldstein, H. W., "The Reaction of Active Nitrogen with Graphite," *Journal of Physical Chemistry*, Vol. 68, No. 1, 1964, pp. 39–41.

[26]Berkowitz-Mattuck, J. B., "Research to Determine the Effects of Surface Catalycity on Materials Behavior in Dissociated Gas Streams-ATJ-Graphite," U.S. Air Force Material Lab., AFML TR-70-172, Arthur D. Little, Inc., Cambridge, MA, Feb. 1970.

T. Lin
Associate Editor